Chapter 4

DFT Calculations for Solid Surfaces

Surfaces are generated when we split a bulk crystal. The created surface is the place where molecules from the gas phase or a liquid come into contact with the material. Atoms at the surface will have a lower coordination than those in the bulk. Due to the changed coordination the surface geometry will relax or possibly even reconstruct, to let surface atoms find their new equilibrium positions. For ideal surfaces of cubic crystals, there are two groups, low Miller index (flat) surfaces, (100), (111) and (110) surfaces, and high Miller index (stepped) surfaces. Stepped surfaces can exhibit significantly different properties compared to flat surfaces due to the effect of the defects. In this chapter, we summarize how to construct a stepped surface model within the context of periodic boundary condition electronic structure calculations, and which geometric and electronic structure quantities of surfaces are evaluated in our analysis.

4.1 Vicinal Surfaces

Close-packed flat surfaces are generated by cutting a fcc bulk along perfect low Miller index planes, like (100) (left panel in Fig 4.1), (111) or (110) surfaces. Although the investigation of such low-index surfaces can generate a wealth of information on surface properties of materials, they are far away from real surfaces. A real surface exhibits additional features like steps, kinks, or vacancies (Fig. 4.1), which can play an important role for the overall surface properties. It is therefore a key endeavor in current surface science to extend our knowledge toward such defects. In our presented work, we focus on atomic step defects. The role of steps can be particularly suitably studied using *vicinal surfaces*, which exhibit a regular array of steps. Cutting a crystal at a small angle (*miscut angle*) away from a low-Miller-index plane creates such *vicinal surfaces* (Fig. 4.2) (or *stepped surfaces* or *high-Miller-index surfaces*). Vicinal surfaces exhibit atomic terraces with a low-index orientation, and these terraces are separated by either straight or kinked atomic steps.

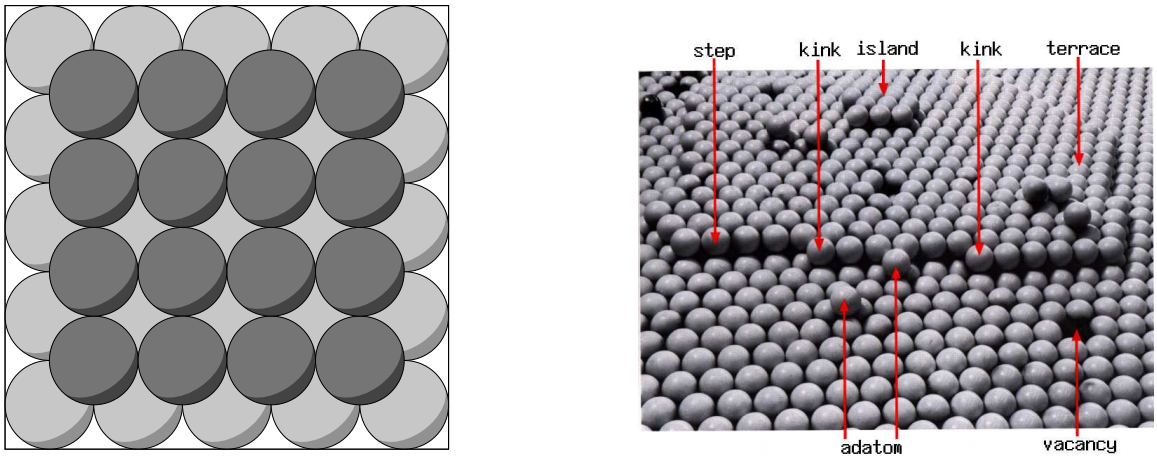

Figure 4.1: Left panel: Top view of a fcc (100) surface (second layer atoms are drawn as light spheres). Right panel: A real surface with steps, kinks, and vacancies.

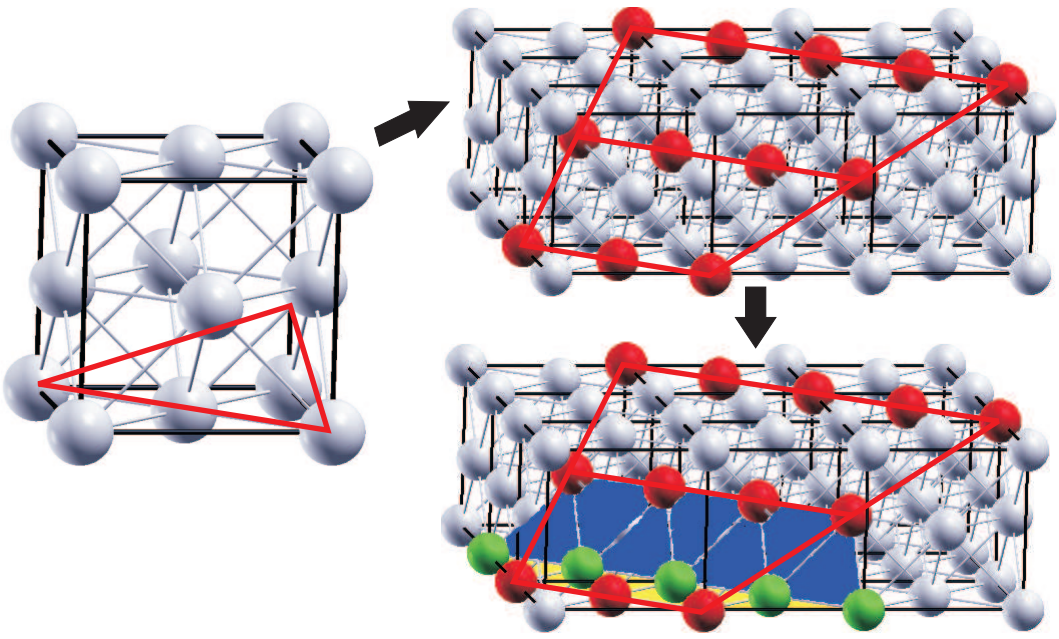

Figure 4.2: Cartoon scheme to create a (113) vicinal surface in a fcc bulk. The left panel is a bulk fcc unit cell. The plane enclosed by red lines is the (113) plane. Expanding the fcc cell 3 times in the x and y directions reveals the (113) plane (top right panel), and atoms on the plane are shown in red color. In the bottom right panel, the yellow plane corresponds to a (100) terrace and the blue one is a (111) step. The green atoms indicate the bottom step edge. The (113) plane can therefore be viewed as two atomic row wide (100) terraces and (111) atomic steps.

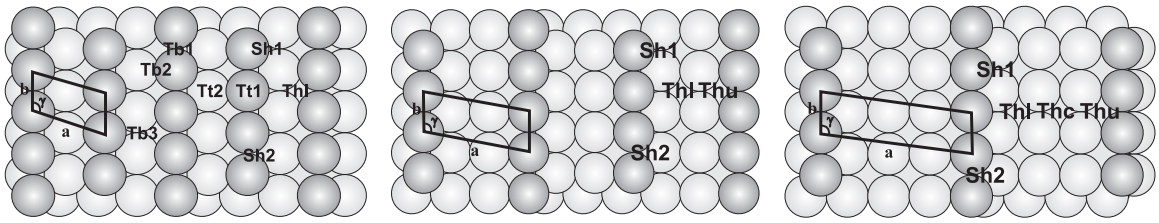

Figure 4.3: Top view of the family of Pd(11N) vicinal surfaces, Pd(113), Pd(115) and Pd(117) (from left panel to right panel). Based on the GGA-PBE bulk fcc Pd lattice constant (3.947 Å), the value of b is same in the three cells, 2.79 Å, and a and γ are 4.83 Å and 106.79^0 for Pd(113), 7.38 Å and 100.89^0 for Pd(115), and 10.06 Å and 97.97^0 for Pd(117), respectively. The additional nomenclatures will be discussed in Chapter 7.

In our work, we focus on Pd(11N) (N=3, 5, 7) vicinal surfaces (Fig. 4.3), which can be built in the way described in Fig. 4.2. The family of Pd(11N) (N=3, 5, 7) vicinal surfaces (top view in Fig. 4.3 and side view in Fig. 7.1) has a similar geometric structure, exhibiting (111) steps and (100) terraces of varying width. There are 2, 3 and 4 atomic rows on the (100) terraces of Pd(113), Pd(115) and Pd(117), respectively. The relationship between the Miller indices of these Pd(11N) vicinal surfaces and their constituent low-index micro-facets becomes clear from the vector decomposition $(11N)=n_{\mathrm{row}}\times(002)+1\times(11\bar{1})$, ($N=2n_{\mathrm{row}}-1$, n_{row}=2, 3, 4...), where n_{row} is the number of atomic rows on the (100) terraces. ($(002)\equiv(100)$ and $(11\bar{1})\equiv(111)$ in cubic symmetry). From the (1×1) surface unit cells of the different vicinal surfaces, Pd(11N) (N=3, 5, 7) indicated in Fig. 7.1, the surface unit cell becomes larger and larger, and the interlayer spacing becomes smaller and smaller with increasing N. Moreover, the larger the surface unit cell, the smaller the atomic density is, and the more open the surface is.

4.2 Surface Models

For surface simulations, there are different models that can be used, most notably the cluster model and the supercell model. Cluster models treat the surface as a small isolated cluster of atoms, one facet of which has the same symmetry and atomic arrangement as the crystal surface intended to study. This model is useful for materials with more localized wavefunctions, such as insulators like MgO [35]. For metal surfaces with de-localized valence wavefunctions, however, it is not suitable, and the supercell model (Fig. 4.4) including slabs and vacua is the more efficient choice. The slab in the supercell is infinite and periodic in the directions parallel to the surface, but finite in the direction perpendicular to the surface.

Such a setup thus enables band formation with the correct dispersions. Two important things should be kept in mind using a supercell model: The vacuum thickness should be large enough to avoid surfaces of consecutive slabs seeing each other, and

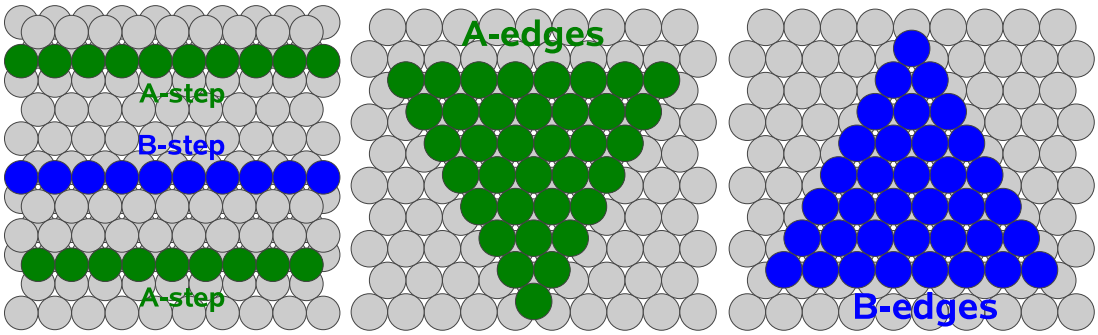

Figure 4.5: Left panel: Striped islands on a fcc(111) surface. The stripes and the valleys between them are both four atomic rows wide. The islands are necessarily bounded by an A (100) (green) and a B (111) (blue) step. Middle and right panels: Two types of triangular islands on an fcc(111) surface, exhibiting (100) (green) and (111) (blue) steps.

the thickness of the slab should also be thick enough to avoid interaction between the two surfaces of one slab. This normally also ensures that the middle layer of the slab exhibits bulk-like properties.

There are three methods to build stepped surfaces in the supercell approach. The first one is a *striped surface* (Fig. 4.5) [38]. Striped surfaces are $(n+1)$ layers thick in cross section through the stripe islands and n layers thick through the trenches in between. On such a striped surface, the disadvantage is that there are necessarily (100) and (111) steps simultaneously present at the two sides of one stripe. The second method to build a stepped surface is via *triangular islands* on the surface (Fig. 4.5) [39]. Such structures contain only one kind of either (100) or (111) steps around each island. This method is useful to differentiate the small energy differences in step formation of (111) and (100) steps, but contains the effect of the step facet edges of the triangle. The third method is via a *slab vicinal surface* as illustrated in Fig. 4.4 and Fig. 7.1. Here, the slab is constructed from the corresponding high Miller-index plane layer by layer. Such a setup allows the investigation of long-range step-step interactions, and also exhibits only one type of step. Additionally, the surface unit cell size is modest. On the other hand, due to the sheared orientation of the supercell, particular care has to be taken to ensure proper **k**-point sampling (Appendix C). The slab vicinal surface model to investigate the properties of vicinal surfaces is used in our study.

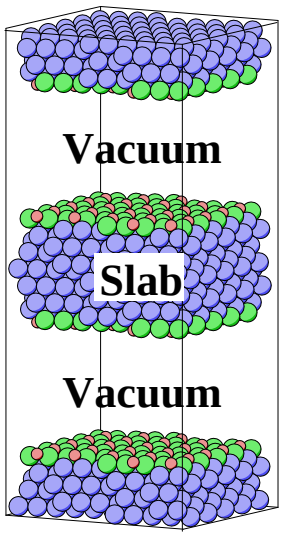

Figure 4.4: Supercell model, including slabs and vacuum.

4.3 Surface Minimization

In surface science surfaces are often classified into three kinds: ideal bulk-truncated surfaces, relaxed surfaces and reconstructed surfaces, depending on how they differ from the same planar termination in the bulk. Assuming cleavage of the crystal does not perturb the remaining material at all and the geometrical arrangement of surface atoms is the same as the bulk termination, a surface is called an *ideal surface*. At a metal surface, the electrons are free to rearrange their distribution in space to lower their kinetic energy (Smoluchowski smoothing [44, 45]), which leads to a net force on the ions. The ensuing movement of the atoms in the surface fringe is called *surface relaxation*. If the atomic movement leads even to a change in the symmetry and size of the surface unit cell (*e.g.* through changing bonds), one talks about *surface reconstruction*. Relaxation changes thus only interlayer spacings, while the surface unit cell does not change at all. Neither flat Pd surfaces, nor Pd($11N$) vicinal surfaces are known to reconstruct so far. Therefore, we focus on the varying interlayer spacings as resulting from surface relaxation,

$$\Delta d_{ij} = 100 \times (d_{ij} - d_{\mathrm{b}})/d_{\mathrm{b}} \quad , \tag{4.1}$$

where d_{b} is the bulk interlayer spacing, and d_{ij} is the interlayer spacing between layers i and j (i and j are the surface layer numbers) after relaxation. With the sign convention behind Eq. 4.1, a minus sign indicates interlayer spacing contraction, while a plus sign indicates expansion. In addition to the varying interlayer spacing, there can be atomic displacements from the bulk position parallel to the surface. Such *registry relaxations* [36], Δr_{ij}, are defined similar to the interlayer relaxation perpendicular to the surface as,

$$\Delta r_{ij} = 100 \times (r_{ij} - r_{\mathrm{b}})/r_{\mathrm{b}} \quad , \tag{4.2}$$

here, r_{b} and r_{ij} are the distance between the positions of two atoms in different layers (i and j) projected onto the surface plane, before and after surface relaxation, respectively. In the registry relaxation, a minus sign means atoms of neighboring layers try to approach each other compared to their bulk distance, while a plus sign means that atoms go further away from each other.

For finding the equilibrium positions of atoms, the PORT minimization method [46], *a reverse-communication trust-region quasi-Newton method* from the Port library, was used to relax the atomic positions. Almost all geometry optimization approaches base on a harmonic approximation, in which the total energy can be expanded near the minimum as,

$$E = E(\mathbf{R}^*) - \mathbf{F}(\mathbf{R}^*) \cdot (\mathbf{R} - \mathbf{R}^*) + \frac{\mathbf{1}}{\mathbf{2}}(\mathbf{R} - \mathbf{R}^*) \cdot \mathbf{H}(\mathbf{R}^*) \cdot (\mathbf{R} - \mathbf{R}^*) \quad , \tag{4.3}$$

where E is the predicted energy for taking a step $\Delta\mathbf{R}$ ($\Delta\mathbf{R}$=$\mathbf{R} - \mathbf{R}^*$) from the current point, $E(\mathbf{R}^*)$ and $\mathbf{F}(\mathbf{R}^*)$ are the energy and force calculated at the current point and

$\mathbf{H}(\mathbf{R}^*)$ is the Hessian matrix. The most straightforward approach is steepest descent, which takes $\mathbf{H}(\mathbf{R}^*)$ as a unitary matrix and takes a step along the direction of the force,

$$\mathbf{F}(\mathbf{R}) = \mathbf{F}(\mathbf{R}^*) - \mathbf{H}(\mathbf{R}^*) \cdot \mathbf{\Delta R} \quad . \tag{4.4}$$

Looking for the minimum of total energy E means searching for a zero of this force. Hence, we have

$$\mathbf{\Delta R} = \mathbf{H^{-1}}(\mathbf{R}^*) \cdot \mathbf{\Delta F}(\mathbf{R}), \quad (\mathbf{\Delta F}(\mathbf{R}) = \mathbf{F}(\mathbf{R}^*) - \mathbf{F}(\mathbf{R})) \quad . \tag{4.5}$$

The left side indicates the finite step $\mathbf{\Delta R}$ which points to the minimum provided the inverse Hessian matrix and quadratic approximation of E are exact. The most important method to investigate this information is the Broyden-Fletcher-Goldberg-Shanno (BFGS) method [47]. The method iteratively builds up an approximation of $\mathbf{H^{-1}}(\mathbf{R}^*)$ by making use of the forces obtained during previous steps of the structure minimization. This Hessian matrix must remain positive definite in order to guarantee that $E(\mathbf{R})$ deceases as we move into the direction $\mathbf{\Delta R}$. If the step $\mathbf{\Delta R}$ is too large, *i.e.* $E(\mathbf{R})$ is increasing, one has to backtrack trying a smaller step along the same direction to get a lower total energy. The minimization process terminates when all atomic forces for a geometry fall below a certain target value.

However, away from the minimum the true Hessian is not necessarily well approximated by this procedure. If the approximated Hessian is not positive definite, the solution to Eq. 4.5 may even be in the uphill direction and the update procedure can go badly wrong. To circumvent this we can rewrite the Eq. 4.4 as,

$$(\mathbf{R} - \mathbf{R}^*)^{\mathbf{T}} \cdot \mathbf{\Delta F}(\mathbf{R}) = (\mathbf{R} - \mathbf{R}^*)^{\mathbf{T}} \cdot \mathbf{H}(\mathbf{R}^*) \cdot (\mathbf{R} - \mathbf{R}^*) \quad . \tag{4.6}$$

If $\mathbf{H}$ is positive definite, the right-hand side is positive, $(\mathbf{R}-\mathbf{R}^*)^{\mathbf{T}} \cdot \mathbf{H}(\mathbf{R}^*) \cdot (\mathbf{R}-\mathbf{R}^*) > \mathbf{0}$. This is called the *curvature condition*. If instead $(\mathbf{R} - \mathbf{R}^*)^{\mathbf{T}} \cdot \mathbf{H}(\mathbf{R}^*) \cdot (\mathbf{R} - \mathbf{R}^*) < \mathbf{0}$ at some stage, precautions have to be taken to prevent the approximated Hessian to become wrong. The PORT method includes such a curvature condition judgment.

Moreover, moving a full step $\mathbf{\Delta R}$ is often not appropriate; it may be too large. One approach would be to search along the direction of $\mathbf{\Delta R}$, but this can be inefficient since it would involve many calculations along a single direction. An alternative approach is to use what is called *Trust-Region* method. Here one calculates the best step for a quadratic model with the current approximation for the Hessian with the additional constraint that $\|\mathbf{\Delta R}\| \leq \mathbf{R}$, where $\mathbf{R}$ is the trust region radius. If a good step is chosen, the current approximation for the Hessian is good and it is safe to increase the radius; if the step is poor (the total energy increases) the radius is decreased. In one word, PORT is still a BFGS type minimization method but with curvature condition and trust region. In the **WIEN2k** code the PORT minimization method is strongly recommended, and for our purposes it proved to be stable, efficient and did not depend too much on the users input. In our surface simulations, the middle layer in the slab is fixed during relaxation procedure, and the remaining layers are fully relaxed until each force component of each atom decreases below 5 mRy/a.u (1 mRy/a.u=7.20 meV/Å).

4.4 Two Key Surface Energetic Properties: γ and E_b

The surface relaxation we just described minimizes the forces on the atoms. Energetically, this relaxation process is suitably characterized by the surface energy per unit area, γ [37]. (For simplicity, it is often just named *surface energy* though.) It is defined as the surface excess free energy per area of a particular crystal facet. The total energy of a surface is,

$$E = TS - pV + \mu N + \gamma A \quad . \tag{4.7}$$

Since γ denotes the cost connected with creating the surface, the most stable surface will minimize γ. In this respect, it also determines the equilibrium shape of a crystal (Wulff construction [40, 41]), or plays a key role in faceting, roughening, crystal growth phenomena, or surface segregation in binary alloys. Most of the experimental data on absolute surface energies [42] comes from surface tension measurement in the liquid phase extrapolated to zero temperature. This procedure includes a rather large degree of uncertainty and corresponds furthermore to an isotropic crystal.

Using a supercell model containing slabs with two equivalent surfaces (*i.e.* a crystal with inversion symmetry), the surface energy, γ at $T = 0$ K of a clean surface, can then be calculated as,

$$\gamma = \frac{1}{2A}(E^\mathrm{total}_\mathrm{slab} - N_s E^\mathrm{total}_\mathrm{bulk}) \quad . \tag{4.8}$$

where $E^\mathrm{total}_\mathrm{slab}$ and $E^\mathrm{total}_\mathrm{bulk}$ are the total energy of the slab and the total energy of a bulk atom, respectively. N_s is the number of atoms in the slab, A is the surface unit area, and the factor $\frac{1}{2}$ is used because the slab has two surfaces.

When atoms or molecules adsorb at surfaces, created bonds with the surface will release energy. The total energy component of this formation energy is called *binding energy*, E_b, which is a function of coverage and distribution of the adsorbates at the surface. In the case of oxygen adsorption, it is written as,

$$E_\mathrm{b} = -\frac{1}{N_\mathrm{O}}\left[E^\mathrm{total}_\mathrm{O/slab} - E^\mathrm{total}_\mathrm{slab} - \frac{N_\mathrm{O}}{2}E^\mathrm{total}_\mathrm{O_2(gas)}\right] \quad . \tag{4.9}$$

Here N_O is the total number of adsorbed O atoms, $E^\mathrm{total}_\mathrm{O/slab}$, $E^\mathrm{total}_\mathrm{slab}$, and $E^\mathrm{total}_\mathrm{O_2(gas)}$ are the total energies of the surface containing oxygen, of the corresponding clean surface, and of an isolated oxygen molecule, respectively. Since a free O_2 molecule is thus used as the zero reference for E_b, a positive binding energy indicates that the dissociative adsorption of O_2 is exothermic at $T = 0\,\mathrm{K}$. To obtain the total energy of the isolated O_2 molecule, we exploit the relation $E^\mathrm{total}_\mathrm{O_2(gas)} = 2E^\mathrm{total}_\mathrm{O(atom)} - D$, where $E^\mathrm{total}_\mathrm{O(atom)}$ is the total energy of an isolated oxygen atom, and D is the theoretical O_2 binding energy. The isolated O atom is then calculated spin-polarized, inside a rectangular cell of side lengths $(12 \times 13 \times 14)$ bohr, Γ-point sampling of the Brillouin zone and without

spherically averaging the electron density in the open valence shell. For D we employ the previously published ultra-converged GGA-PBE value of 6.202 eV. [96] Compared to the experimental binding energy of 5.12 eV [110], this value shows the well-known, substantial GGA-induced error. With this value Eq. 4.9 can be rewritten as,

$$E_{\mathrm{b}} = -\frac{1}{N_{\mathrm{O}}}(E^{\mathrm{total}}_{\mathrm{O/slab}} - E^{\mathrm{total}}_{\mathrm{slab}}) + (E^{\mathrm{total}}_{\mathrm{O(atom)}} - 3.101\,\mathrm{eV}) \quad . \tag{4.10}$$

4.5 Step Formation Energy

The change in the $T = 0$ K surface energies of vicinal surfaces compared to the corresponding terrace surface energies reflects the additional cost due to the atomic steps at the surface. This cost can be expressed by the so-called *step formation energy* [48, 49]. Consider a vicinal surface (Fig. 4.6) exhibiting a periodic succession of terraces with equal widths, separated by steps of monoatomic height. The step energy density (step formation energy per unit length) $\bar{\beta}$ of the vicinal surface is defined by the equation:

$$\bar{\beta} = \beta(\mathbf{n})b - \beta(\mathbf{n_0})s \quad . \tag{4.11}$$

So,

$$\begin{aligned} \beta(\mathbf{n}) &= \beta(\mathbf{n_0})\frac{s}{b} + \frac{\beta(\theta)}{b} \\ &= \beta(\mathbf{n_0})\cos\theta + \bar{\beta}\sin\alpha/h \quad , \end{aligned} \tag{4.12}$$

where $\beta(\mathbf{n})$ and $\beta(\mathbf{n_0})$ is the surface energy (per unit length) of the vicinal surface and the flat terrace surface, respectively. This equation yields the surface energy of vicinal surfaces in terms of the step energy density $\bar{\beta}$. On the other hand, it is useful to consider the step formation energy E_{step} per step atom rather than the energy density $\bar{\beta}$, $E_{\mathrm{step}} = \bar{\beta}a_0$. Then Eq. 4.12 can be rewritten as,

$$\begin{aligned} E_{\mathrm{step}} &= (\beta(\mathbf{n}) - \beta(\mathbf{n_0})\cos\theta)\frac{a_0 h}{\sin\theta} \\ &= (\beta(\mathbf{n}) - \beta(\mathbf{n_0})\cos\theta)a_0 b \\ &= \gamma_{\mathrm{vicinal}}(\mathbf{n}) - (n_{\mathrm{row}} - 1)\beta(\mathbf{n_0})\mathbf{a_0}\mathbf{b_0} \\ &= \gamma_{\mathrm{vicinal}}(\mathbf{n}) - (n_{\mathrm{row}} - 1)\gamma_{\mathrm{terrace}}(\mathbf{n_0}) - f\gamma_{\mathrm{terrace}}(\mathbf{n_0}) \quad , \end{aligned} \tag{4.13}$$

where $\gamma_{\mathrm{vicinal}}(\mathbf{n})$ and $\gamma_{\mathrm{terrace}}(\mathbf{n_0})$ are the surface energies per atom of the vicinal surface and flat surface, respectively. n_{row} is the number of atomic rows at terraces. The additional term, $f\gamma_{\mathrm{terrace}}(\mathbf{n_0})$, is a correction for the fact that the step may not rise at a right angle from the terrace. f is a geometrical factor explained in Fig. 4.6. The values for f on different vicinal surfaces can be found in ref. [48]; f=1/2 for the ideal vicinal Pd(11N) surfaces, n_{row}(100)+(111).

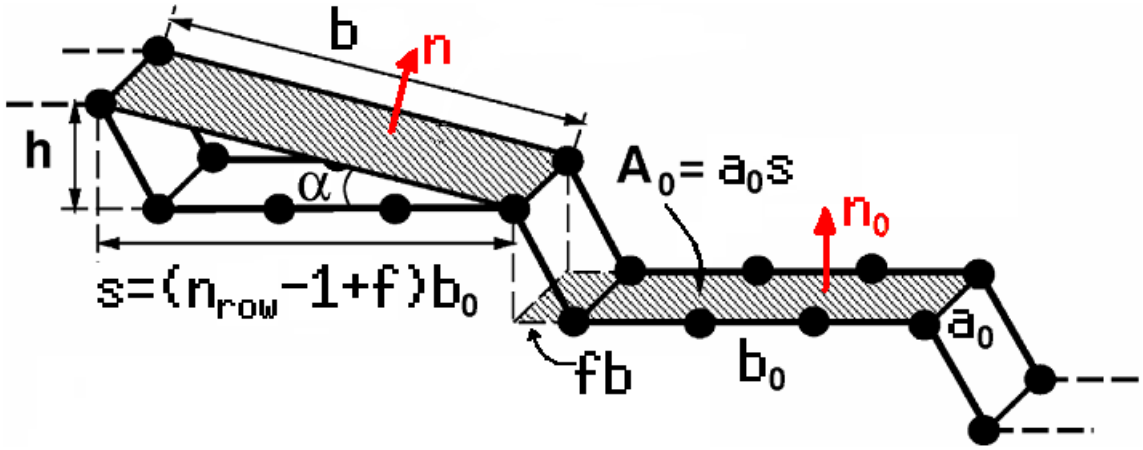

Figure 4.6: Model explaining the geometrical view behind Eq. 4.13. $\mathbf{n}$ and $\mathbf{n}_0$ are the directions normal to the vicinal surface and to the terraces, respectively. b is the distance between two consecutive steps, b_0 is the distance between two consecutive atomic rows in a terrace. a_0 is the unit along the step edge. α is the miscut angle and n_{row} is the number of atomic rows, f is a geometrical factor depending on the vicinal surface and h is the height of the steps.

4.6 Local Density of States (LDOS)

The local density of electronic states (LDOS), which is the number of electronic states within energy between E and $E + dE$, is an important quantity to analyze the electronic structure. It is defined as,

$$n(\mathbf{r}, \epsilon) = \sum_{i=1}^{\infty} |\varphi_i(\mathbf{r})|^2 \delta(\epsilon - \epsilon_i) \quad , \tag{4.14}$$

where $\varphi_i(\mathbf{r})$ is the single-particle eigenfunction of the Kohn-Sham Hamiltonian, and ϵ_i is the corresponding eigenvalue. The LDOS exhibits system properties, such as the valence band, conduction band, Fermi energy, bonding region, *etc.* Based on that, we can determine whether the system is a metal, or insulator or semiconductor. In the LAPW method, the muffin-tin sphere is a convenient *local* region to calculate the LDOS of different states projected onto the different atoms. Fig. 4.7 shows the correspondingly computed LDOS of fcc bulk Pd. The valence d-band is nicely discerned and the Fermi-level falls at the upper edge, indicating the high filling characteristic for this late transition metal (TM).

4.7 Surface Core-level Shifts

Apart from the LDOS, surface core-level shifts (SCLS) [50] are another important quantity that can be used to investigate the electronic structure of surfaces. Although the core orbitals do not take part in the bonding, they are affected by changes in the

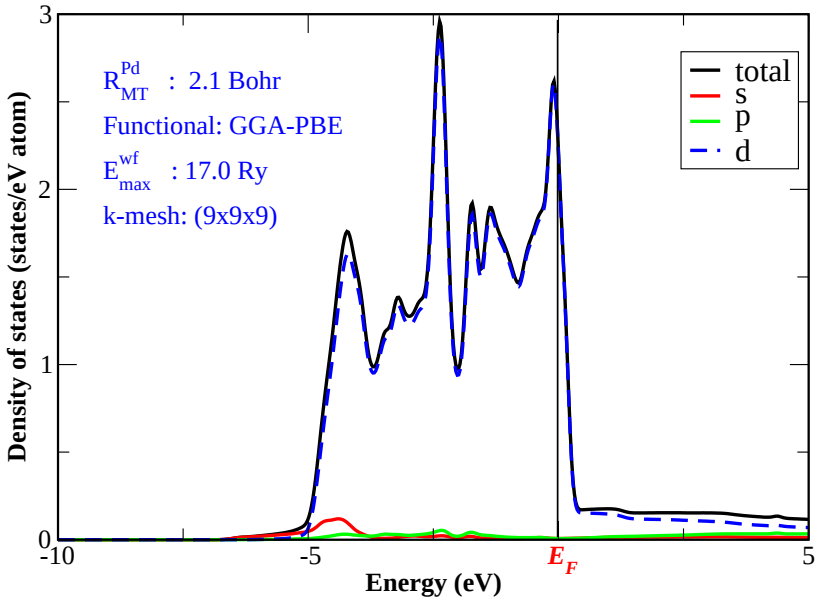

Figure 4.7: Local density of states of bulk fcc Pd (projected onto s, p and d atomic orbitals). s and p orbitals have a very small contribution to the total valence DOS, while the Pd $4d$ band is clearly visible. The Fermi level is at its upper end of this band, reflecting the position of Pd in the periodic system of elements.

atomic environment, and as such the core level energies are sensitive local probes of changes in the electronic structure in different environments. Core level energies can be measured for both clean and adsorbate-covered surfaces by high resolution core-level photoemission spectroscopy [52]. The SCLS [51], Δ^{SCLS}, is defined as the difference in energy that is needed to remove a core electron either from the surface or from a bulk atom,

$$\Delta^{\mathrm{SCLS}} = [E_{\mathrm{surface}}(n_c - 1) - E_{\mathrm{surface}}(n_c)] - [E_{\mathrm{bulk}}(n_c - 1) - E_{\mathrm{bulk}}(n_c)] \quad , \tag{4.15}$$

where $E_{\mathrm{surface(bulk)}}(n_c)$ is the total energy of the system considered as a function of the number of electrons n_c in a particular core level c of a surface or bulk atom, respectively. In DFT calculations, we can rewrite Eq. 4.15 approximately as,

$$\Delta^{\mathrm{SCLS}}_{\mathrm{initial}} = [\epsilon^c_{\mathrm{bulk}} - \epsilon^F_{\mathrm{bulk}}] - [\epsilon^c_{\mathrm{surface}} - \epsilon^F_{\mathrm{surface}}] \quad , \tag{4.16}$$

where, $\epsilon^c_{\mathrm{surface(bulk)}}$ is the KS eigenvalue of the core level c in the surface and bulk, respectively. $\epsilon^F_{\mathrm{surface(bulk)}}$ is the Fermi level in the surface and bulk, respectively. In this SCLS approximation, $\Delta^{\mathrm{SCLS}}_{\mathrm{initial}}$ is one contribution to the measurable SCLS in x-ray photoemission spectroscopy (XPS), where the latter comprises in addition also the screening contribution of the valence electrons in response to the created core hole [50]. For a meaningful comparison with the experimental data, a total SCLS taking

both initial and final state screening effects into account must be used. However, it is not so much this connection to an experimentally accessible quantity that makes us interested in the initial-state SCLS in this work, but rather that the $\Delta^{\mathrm{SCLS}}_{\mathrm{initial}}$ are a very sensitive probe of changes in the local electronic structure of an atom in different environments, which is why we mostly content ourselves here with focusing on the $\Delta^{\mathrm{initial}}_{\mathrm{SCLS}}$ of the $3d$ Pd core level.

In Fig. 4.9, one can see for both clean Pd(111) and Pd(100) that the $4d$ band of the first layer atoms is narrower than those of the deeper lying surface layers. This can be rationalized as follows: The width of the band depends on the overlap or hybridization of orbitals with orbitals from neighboring atoms. The higher the coordination, the more overlap and the broader the band. The reduced coordination of the surface atoms leads therefore to a narrowing of the valence d-band. Moreover, because the total number of valence states must be conserved, the narrowed LDOS is enhanced around the Fermi level. In order to keep local charge neutrality, the Pd d-band is therefore also slightly shifted to a higher energy (Fig. 4.8), which induces a positive surface potential shift $[\Delta V(r) = V_{\mathrm{surface}}(r) - V_{\mathrm{bulk}}(r)]$ [51, 53]. Since $\Delta V(r)$ is related with the initial-state SCLS (Δ): $\Delta_{3d} \approx -\int dr \Delta V(r) r^2 |R_{3d}(r)|^2$, the changed potential acting on the Pd surface atom $3d$ core levels generates a negative initial surface core level shift. This would be reversed for surface atoms in an early TM (less than half full d band), where the surface potential shift is negative and a positive $3d$ initial-state surface core level shift is induced. The computed initial-state surface core level shift of the $3d$ level is -0.39 eV and -0.50 eV for the outermost layer of Pd(111) and Pd(100) (with GGA-PBE), respectively. They are therewith much larger than those of the other deeper lying layers, which are nearly zero. Both the LDOS and the SCLS reflect therefore the efficient metallic screening behavior of Pd: Only the first layer atoms are largely affected by the changed coordination and exhibit correspondingly significantly changed parameters. These changes are rapidly screened away by the mobile conduction electrons deeper inside the crystal, and already the 2nd and lower layer atoms approach properties virtually indistinguishable from the ones of bulk atoms. The LDOS of the middle layer atoms in the slab is correspondingly already quite similar to the bulk LDOS (Fig. 4.7).

In additional to the initial SCLS, we need to compute the total SCLS including the final SCLS contribution for comparing with the experimental value. We already know that the final SCLS is induced by the valence screen effect on the creating core in the core level. The screen effect in the energy different in Eq. 4.15 can be determined by the mean value theorem of integration [51],

$$E(n_c - 1) - E(n_c) = \int_{n_c}^{n_c - 1} \frac{\partial E(n')}{\partial n'} dn' \approx -\epsilon_c (n_c - 1/2) \quad . \tag{4.17}$$

In order to implement the final state effect by the DFT calculation, we ionize the interesting core level of atoms by moving 1/2 electron from the core to the valence band.

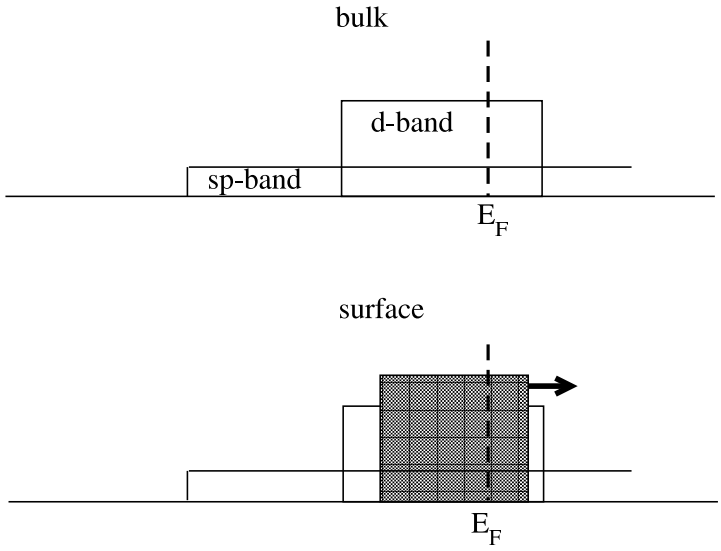

Figure 4.8: Cartoon using the rectangular d-band model to illustrate the d-band surface shift in late TM (more than half full d band). In order to maintain the same number of occupied states up to E_F, the narrowed surface band (dash shading) shifts up in energy.

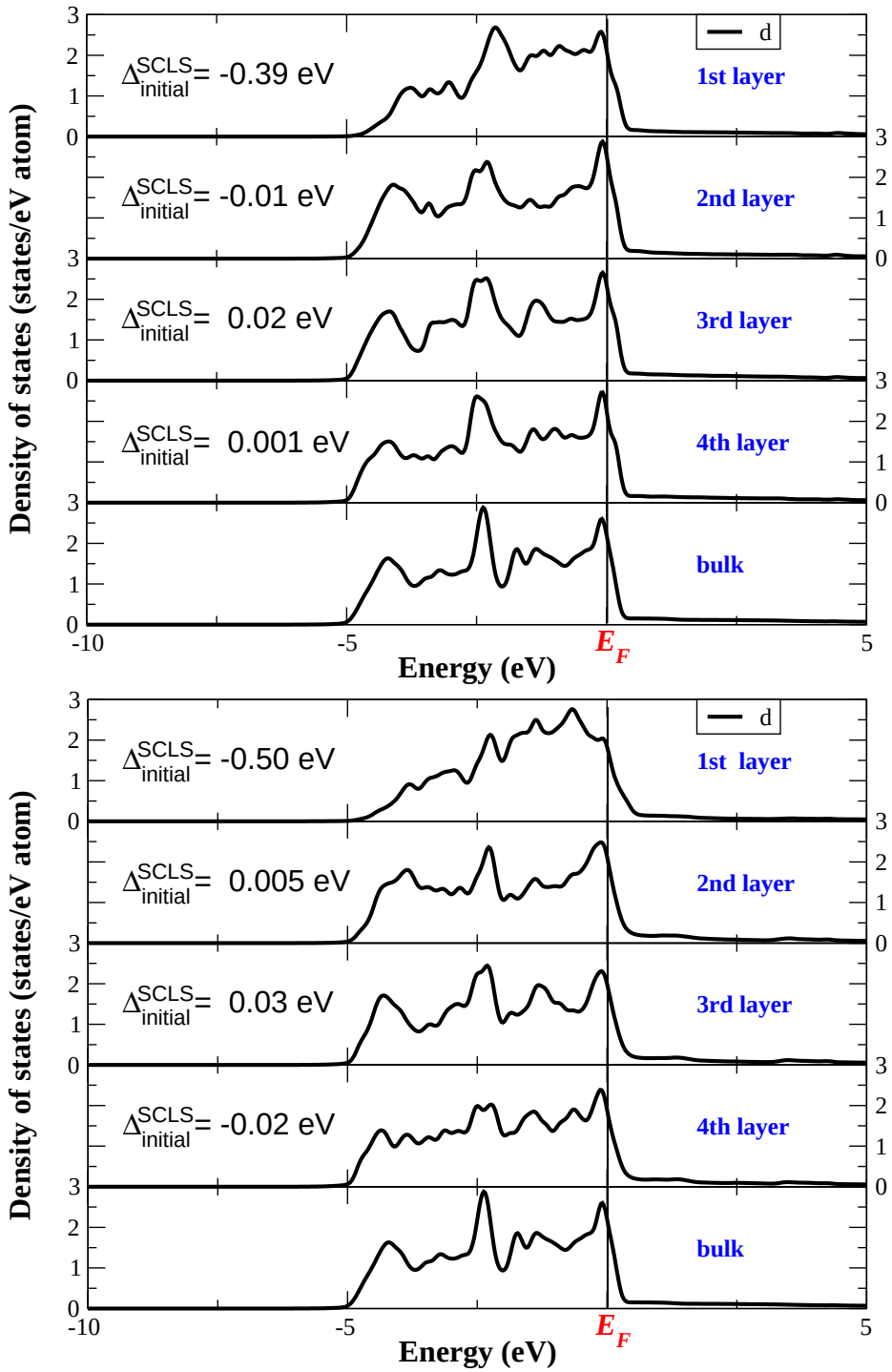

Figure 4.9: Local density of states of different layers for Pd(111) [top panel] and Pd(100) [bottom panel]. The LDOS of the outermost layer is significantly narrower than those of the other layers, while the LDOS of the middle layer is already similar to the bulk DOS. Additionally shown are the $3d$ initial-state surface core level shifts $\Delta^{\mathrm{SCLS}}_{\mathrm{initial}}$ of the corresponding layers.